

PAPER

## Thickness-dependent surface plasmon resonance of ITO nanoparticles for ITO/In-Sn bilayer structure

To cite this article: Wenzuo Wei *et al* 2018 *Nanotechnology* **29** 015705

View the [article online](#) for updates and enhancements.

### Related content

- [Plasmonic characteristics of Ag and ITO/Ag ultrathin films as-grown by sputtering at room temperature and after heating](#)  
C Guillén and J Herrero
- [Engineering metallic nanostructures for plasmonics and nanophotonics](#)  
Nathan C Lindquist, Prashant Nagpal, Kevin M McPeak *et al.*
- [A sharp and visible range plasmonic in heavily doped metal oxide films](#)  
Uma Nerle, R M Hodlur and M K Rabinal



**IOP | ebooks™**

Bringing you innovative digital publishing with leading voices to create your essential collection of books in STEM research.

Start exploring the collection - download the first chapter of every title for free.

# Thickness-dependent surface plasmon resonance of ITO nanoparticles for ITO/In-Sn bilayer structure

Wenzuo Wei<sup>1</sup> , Ruijin Hong<sup>1,2</sup>, Ming Jing<sup>1</sup>, Wen Shao<sup>1</sup>, Chunxian Tao<sup>1</sup> and Dawei Zhang<sup>1</sup>

<sup>1</sup>Engineering Research Center of Optical Instruments and Systems, Ministry of Education and Shanghai Key Lab of Modern Optical Systems, University of Shanghai for Science and Technology, No. 516 Jungong Road, Shanghai 200093, People's Republic of China

<sup>2</sup>State Key Laboratory of Applied Optics, Changchun Institute of Optics, Fine Mechanics and Physics, Chinese Academy of Sciences, Changchun 130033, People's Republic of China

E-mail: [rjhong@usst.edu.cn](mailto:rjhong@usst.edu.cn)

Received 19 September 2017, revised 8 November 2017

Accepted for publication 15 November 2017

Published 5 December 2017



CrossMark

## Abstract

Tuning the localized surface plasmon resonance (LSPR) in doped semiconductor nanoparticles (NPs), which represents an important characteristic in LSPR sensor applications, still remains a challenge. Here, indium tin oxide/indium tin alloy (ITO/In-Sn) bilayer films were deposited by electron beam evaporation and the properties, such as the LSPR and surface morphology, were investigated by UV–VIS–NIR double beam spectrophotometer and atomic force microscopy (AFM), respectively. By simply engineering the thickness of ITO/In-Sn NPs without any microstructure fabrications, the LSPR wavelength of ITO NPs can be tuned by a large amount from 858 to 1758 nm. AFM images show that the strong LSPR of ITO NPs is closely related to the enhanced coupling between ITO and In-Sn NPs. Blue shifts of ITO LSPR from 1256 to 1104 nm are also observed in the as-annealed samples due to the higher free carrier concentration. Meanwhile, we also demonstrated that the ITO LSPR in ITO/In-Sn NPs structures has good sensitivity to the surrounding media and stability after 30 d exposure in air, enabling its application prospects in many biosensing devices.

Keywords: localized surface plasmon resonance, LSPR sensitivity, LSPR stability, plasmonic materials

(Some figures may appear in colour only in the online journal)

## 1. Introduction

Large local electromagnetic field enhancements induced by collective electron oscillations in metallic nanoparticles (NPs) will occur when the resonance frequency of the conduction electrons and incident light are matched, known as localized surface plasma resonance (LSPR) [1, 2]. There has been a focus on research in LSPR for many years because of its potential applications in photonics and optoelectronics devices, such as surface-enhanced Raman scattering [3, 4], photothermal therapy [5], light harvesting in solar cells [6], plasmon-enhanced fluorescence [7], nonlinear optics [8],

photoluminescence and photonic devices [9–11]. In particular, metallic NPs have been extensively used as photothermal transducing agents in biomedical applications due to their strong absorption in near-infrared region (NIR) [12–14]. Using NIR light as a remote stimulus, photothermal therapy exploits the local heating effect to selectively ablate cancerous tissue or kinetically drive local chemical processes while minimizing adverse side effects [15–17]. Due to the lack of small-sized photosensitive materials that exhibit strong absorption and high photothermal transduction efficiency in NIR, NIR light is seldom applied in photothermal therapy [18, 19]. The intensity and efficiency are affected by many

factors. Of great importance is the tunability and extension of the LSPR wavelength, which is determined by the size, shape and composition as well as the surrounding medium of metallic NPs. The fine LSPR tunability from the visible to the NIR or from NIR to the infrared range (IR) can be achieved by changing these factors appropriately. Commonly used plasmonic materials, such as gold and silver, have been demonstrated to show LSPR in the visible–NIR region. However, there are still restrictions in the realization of plasmonic devices due to the high loss and limited tunability of the carrier density in these noble metal materials [20]. In addition, the conducting metal oxides, whose LSPR is phenomenologically the same as that observed in the noble metals, will contribute significantly to plasmon science applications, because the use of high-cost noble metals will no longer be required [21]. Thus, it is of great significance to develop cost-effective plasmonic materials with low loss and fine LSPR tunability.

Recently, doped semiconductor NPs have been demonstrated to exhibit well-tunable LSPR features that are not readily available in noble metals [21–24]. Although the LSPR of noble metal nanostructures has been intensively studied for its ability to enhance the local field, so far few studies have utilized it when sustained by heavily doped semiconductors as near-field nanoantennas [25]. There are a few reports on the plasmonic coupling between metal and nanostructures [12] and semiconductors, while a lot of work has focused on noble metal NPs [26–29]. Among doped semiconductors, indium tin oxide (ITO) would be the desired plasmonic material candidate, because the high carrier density in ITO makes it suitable for realizing a tunable LSPR wavelength in the NIR region. It is known that the LSPR of ITO NPs can theoretically be tuned from the ultraviolet to infrared wavelength regions by varying the electron density from  $10^{23}$  to  $10^{19}$   $\text{cm}^{-3}$ . Typically, the LSPR wavelength of ITO NPs in the NIR region can be tuned by adjusting the concentration of free charge carriers through chemical or electrochemical doping [25, 30, 31]. For example, Kanehara *et al* [21] synthesized ITO NPs with good LSPR by changing the Sn doping concentrations, and Garcia *et al* [23] realized the tunable LSPR of ITO by the post-synthetic electrochemical modulation of the electron concentration. However, in terms of the preparation process of ITO, they are not only complicated but also time-consuming. Moreover, the process of depositing ITO NPs generates chemical and metal waste, which significantly hinders the cost competitiveness and environmental friendliness of the mass production of plasmonic devices and applications. Therefore, a new way that can both improve the deposition efficiency and quality is essential.

Since LSPR tunability is sensitive to the surrounding medium, dielectric/metal double layer structures such as ITO/Ag and ITO/Au have been studied for years and are propitious for good tunability at the LSPR wavelength [32–34]. To date, however, little is known about the properties of ITO/In-Sn bilayer structures, and the corresponding LSPR phenomenon has not been reported. To tune the LSPR wavelength of ITO NPs, we herein propose an ITO/In-Sn

bilayer structure and find very good tunability with enhanced intensity. The LSPR wavelength of ITO NPs can be well tuned over a wider range by simply engineering the thickness of ITO/In-Sn NPs without any microstructure fabrications. In addition, the thermal annealing method was carried out to tune the LSPR of the samples. Moreover, both the stability and sensitivity of the LSPR of ITO NPs were investigated in this paper. Our findings may open up a new way of realizing fine ITO LSPR tunability and fulfil its practical application in biosensing devices.

## 2. Material and methods

Prior to deposition, K9 glass substrates were ultrasonically cleaned in acetone, ethanol and deionized water for 20 min, respectively, and were subsequently dried with a flow of nitrogen. In-Sn alloy thin films and ITO layers were successively deposited by electron beam evaporation from indium tin alloy (99.99%) and sintered ITO ceramics (99.99%) containing 10 wt.%  $\text{SnO}_2$ , respectively. The chamber was evacuated to a base pressure of less than  $8.0 \times 10^{-4}$  Pa. ITO layers with thicknesses of 50, 80, 110, 140 and 170 nm were used in different experimental groups; each group has four samples with In-Sn thin films deposited with 3, 5, 7 and 10 nm, respectively. The thickness of both layers was monitored by an *in situ* quartz crystal microbalance. To guarantee the uniformity of the film thickness, all substrates were set on the fixture with the same circle radius. All annealing experiments were carried out at 200 °C, 300 °C and 400 °C respectively on the same system used for depositing bilayers. The pressure was  $7.0 \times 10^{-4}$  Pa and the annealing time was maintained at 20 min. The samples were also deposited with a  $\text{TiO}_2$  layer to figure out the effect of the refractive index of the surrounding medium on the LSPR. To better understand the whole process, a schematic of the experimentation is shown in figure 1.

The structural properties and the crystallinity of the samples were analyzed by x-ray diffraction (XRD) using a Rigaku MiniFlex600 system, with  $\text{Cu } k\alpha$  radiation ( $\lambda = 0.15408$  nm). The optical absorption spectrum of the samples was measured by using an ultraviolet–visible–near-infrared (UV–VIS–NIR) double beam spectrophotometer (Lambda 1050, Perkins Elmer, USA). The surface morphology was characterized with atomic force microscopy (AFM) (XE-100, Park System). All the measurements were carried out at room temperature.

## 3. Results and discussion

### 3.1. The crystal structure and composition of ITO/In-Sn bilayer film

Figure 2 reveals the XRD patterns of the ITO/In-Sn bilayer films prepared at room temperature by electron beam evaporation. In both single In-Sn layers and ITO/In-Sn bilayers, there are two diffraction peaks at around  $32.8^\circ$  and  $69.2^\circ$  in

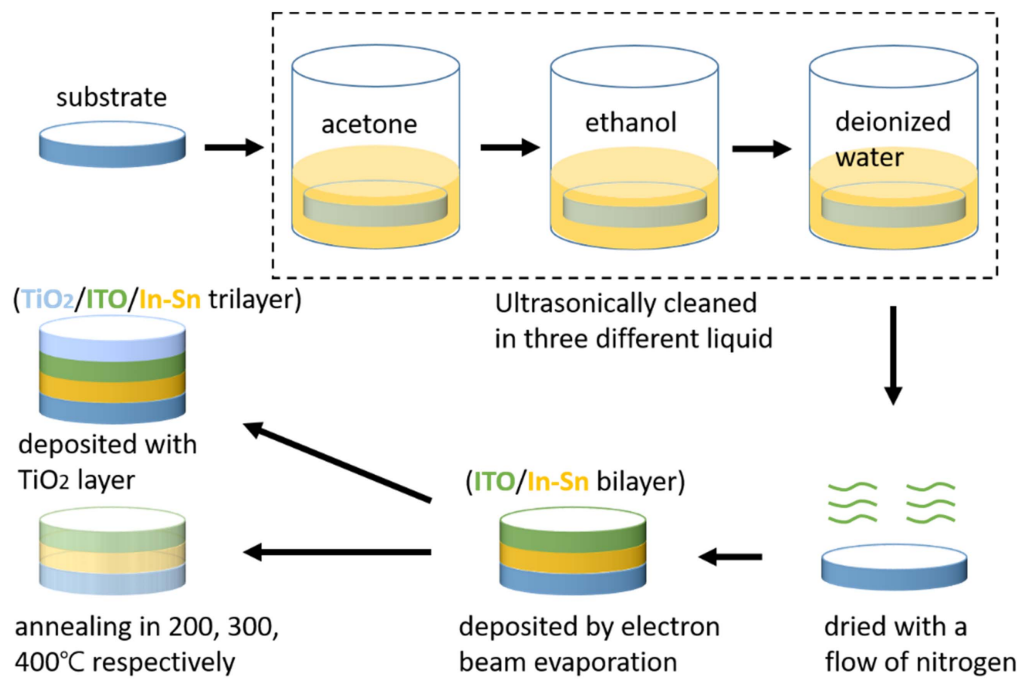
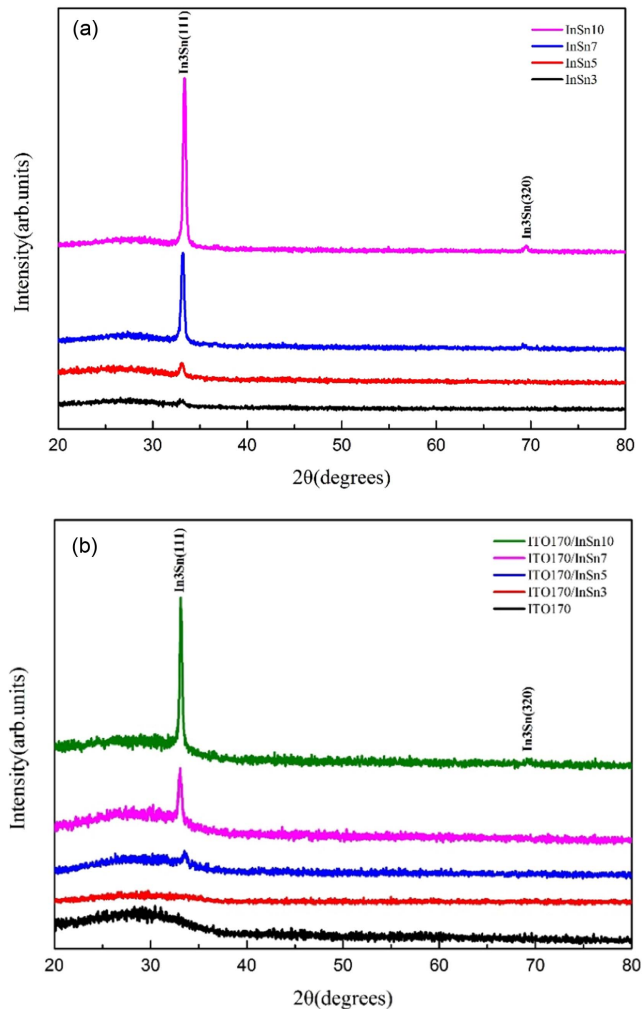


Figure 1. A schematic diagram of the whole experiment.

the pattern, which correspond to the (111) and (320) peaks of In<sub>3</sub>Sn, respectively. No diffraction from randomly oriented grains or impurity phases can be observed from the x-ray pattern, as confirmed by the standard card (JCPDS:07-0345). For the as-deposited In-Sn samples without the ITO layer (as shown in figure 2(a)), the intensities of both diffraction peaks are enhanced as the thickness of the In-Sn layer increases. The strongest peak at approximately 32.8° corresponds to the (111) crystallographic plane, indicating the preferential orientation of pure In-Sn grains along the (111) crystallographic direction. In general, for non-epitaxial deposition on a substrate, the surface of the film tends to be either a (111) or a (0001) plane, because these planes exhibit minimum surface free energies [35]. This means that the (111) textured film must form in an effective equilibrium state, where enough surface mobility is given to impinging atoms under a certain deposition condition [36]. For ITO/In-Sn bilayers, however, the XRD intensity of the In-Sn film decreases when compared to that of pure In-Sn alloy film on a K9 substrate because of the grain boundary in the interface between the surface of the In-Sn and ITO layer. Note that pure ITO film deposited at room temperature is amorphous from the XRD pattern (black line, figure 2(b)). A similar observation was also noticed by other studies [37, 38]. An amorphous structure can also be observed for the sample of ITO(170 nm)/In-Sn(3 nm) due to the very thin thickness of the In-Sn layer and the protection of the ITO layer, which cannot be easily detected by XRD (red line, figure 2(b)). For the sample of ITO(170 nm)/In-Sn(5 nm) (blue line, figure 2(b)), note that the (111) peak is shifted to higher  $2\theta$  angles compared to the other two samples with thicker In-Sn thicknesses (purple and green lines, figure 2(b)), as a result of the partial relief of the intrinsic stress within the films.

### 3.2. AFM images of ITO/In-Sn bilayer films

Figure 3 shows the representative AFM images and their corresponding grain height distributions (as shown in the right column) of ITO/In-Sn NPs with increasing ITO and the same In-Sn thickness. Significant changes in the morphologies of ITO/In-Sn NPs are found to be closely related to the ITO thickness. Without the ITO layer, the single In-Sn layer is grown with small, sharp NPs, which are shown to have the lowest height (around 10 nm) and the smallest root-mean-square roughness (RMS, 3.220 nm). After being covered with the ITO layer (50 and 80 nm), the ITO/In-Sn NPs are evenly distributed and consist of grains with spherical and ellipsoidal shapes. Accordingly, the RMSs are nearly constant (4.235 and 4.543 nm respectively), and so are their grain height distributions, as shown in the right column. With a thicker ITO deposition, the surface morphology changes noticeably: the surface becomes rougher with an increasing RMS and nonuniform, large-grained NP distributions. Obviously, the average grain size is larger after thicker ITO deposition. In LSPR, it is known that the strength of plasmonic coupling depends on both the size and shape of the metallic NPs [39–41]. A small variation in the size of the NPs will cause a shift in the coupling between them [42]. Due to the larger ITO/In-Sn NPs, the coupling between the ITO NPs and In-Sn NPs will be more pronounced, resulting in a stronger LSPR phenomenon, thereby generating the difference for its optical absorption (figure 4) [43]. Combined with the absorption spectrum discussed in the next section 3.3, our experimental results demonstrate that the deposition of an ITO layer on top of the In-Sn NPs can distinctly tune both the In-Sn and the ITO LSPR wavelength. Thus, we expect the ITO layer to be able to induce a higher surface area (and thus higher sensitivity) for LSPR sensor applications.



**Figure 2.** The representative XRD patterns of (a) the single In-Sn layer and (b) the ITO/In-Sn bilayer films.

### 3.3. The LSPR of ITO NPs in the NIR region of the ITO/In-Sn structure

The UV–VIS–NIR absorption spectra indicating the different thicknesses of the ITO/In-Sn structure are shown in figure 4. For a single In-Sn thin film (as shown in figure 4(a)), an absorption peak appears at around 200–300 nm, corresponding to the intrinsic absorption peak of the In-Sn film, which has been demonstrated in our previous work [44]. When the In-Sn NPs are clad with a thin ITO layer of 50 nm or 80 nm, the absorption peak is located in the visible wavelength region (figures 4(b) and (c)). This is expected to correspond to the absorption peak of the In-Sn alloy thin film. The absorption intensity is enhanced with the absorption peak red-shifting gradually, as shown in figure 4(b). When the ITO thickness is 80 nm, the LSPR phenomenon of the In-Sn NPs is more obvious: its LSPR wavelength red-shifts distinctly (from 514 to 818 nm). Interestingly, however, two separate LSPR phenomena can be observed in the absorption spectrum, when In-Sn NPs are clad with thicker ITO layers of 110, 140 and 170 nm, respectively (figures 4(d)–(f)). Based on the above, it can be concluded that the absorption peaks at a short wavelength and those at a long wavelength correspond

to the LSPR absorption peak of In-Sn and ITO NPs [20, 21], respectively. The LSPR wavelength shift of In-Sn NPs with an ITO thickness of over 110 nm is more obvious than that with less than 80 nm: the LSPR absorption peak shifts from 363 to 750 nm as the ITO thickness increases from 110 to 170 nm. It is well known that the LSPR wavelength not only depends on the film thickness, but also on other deposition parameters, which decide the shape and size of the nanostructures in the film [1, 2, 9, 10]. The presence of the ITO layer is expected to result in the strong localization of the field at the ITO/In-Sn interface and a drastic field enhancement, especially with full electric contact and strong interactions in the dielectric/metal nanostructures [45].

In addition to that of In-Sn NPs, the LSPR phenomenon of ITO NPs is also notable in the study. We find that the absorption resonance of ITO only starts to peak in the NIR region when In-Sn NPs are clad with thicker ITO layers (over 110 nm), as shown in figures 4(b)–(c). For samples with ITO thicknesses of 110 nm, the absorption peak can be well tuned from the NIR to the IR region: the absorption peak shows a red shift from 858 to 1118 nm as the In-Sn film thickness increases from 3 to 10 nm. Further increasing the ITO thickness to 140 and 170 nm, both LSPR peaks undergo an obvious red shift from 1104 to 1448 nm and from 1388 to 1758 nm, respectively. The absorption peak of ITO NPs gets sharper and more intense simultaneously in the process of red shifting to a longer wavelength. To better understand the effect of thickness on the LSPR of ITO, the LSPR wavelength shift as a function of the In-Sn alloy film is plotted in figure 5: the LSPR wavelength peak of ITO shows a similar gradual red shift with an increasing In-Sn thickness for the fixed ITO layer thickness. Also, for a fixed In-Sn NPs thickness, the absorption peak increases with the ITO thickness. It is reported that ITO NPs with shorter absorption wavelengths have higher free-electron densities [20, 21]. In the electronic structure of the ITO film, the Sn atom that replaces an In atom results in a single free electron. Therefore, the ITO(170 nm)/In-Sn films are expected to have the lowest free electron density of the studied ITO NPs, resulting in the lower LSPR frequency [46], as shown in figure 5. On the other hand, it is known that plasmonic coupling takes place when the layers are close to each other, and therefore, the plasmon resonance of each layer is affected by the plasmon resonance of its neighboring layer. The strength of plasmonic coupling depends on the surface layer (ITO) thickness and the incident light as well as the dielectric constant. As discussed in the AFM results (section 3.2), the small variation of the interface between the metal film and the dielectric layer will cause a shift in the electric field density on the surface, resulting in a change of the electron oscillation frequency, thereby generating different cross-sections for its optical properties including absorption [47, 48]. As a result, the small interface between layers causes a small change of the surrounding medium, resulting in a red shift and making the LSPR absorption peak shift smaller, as shown in figure 4. In addition, it should be noted that the band of In-Sn in the LSPR absorption spectrum is sharper and more intense, which indicates that the resulting LSPR sensor can achieve good

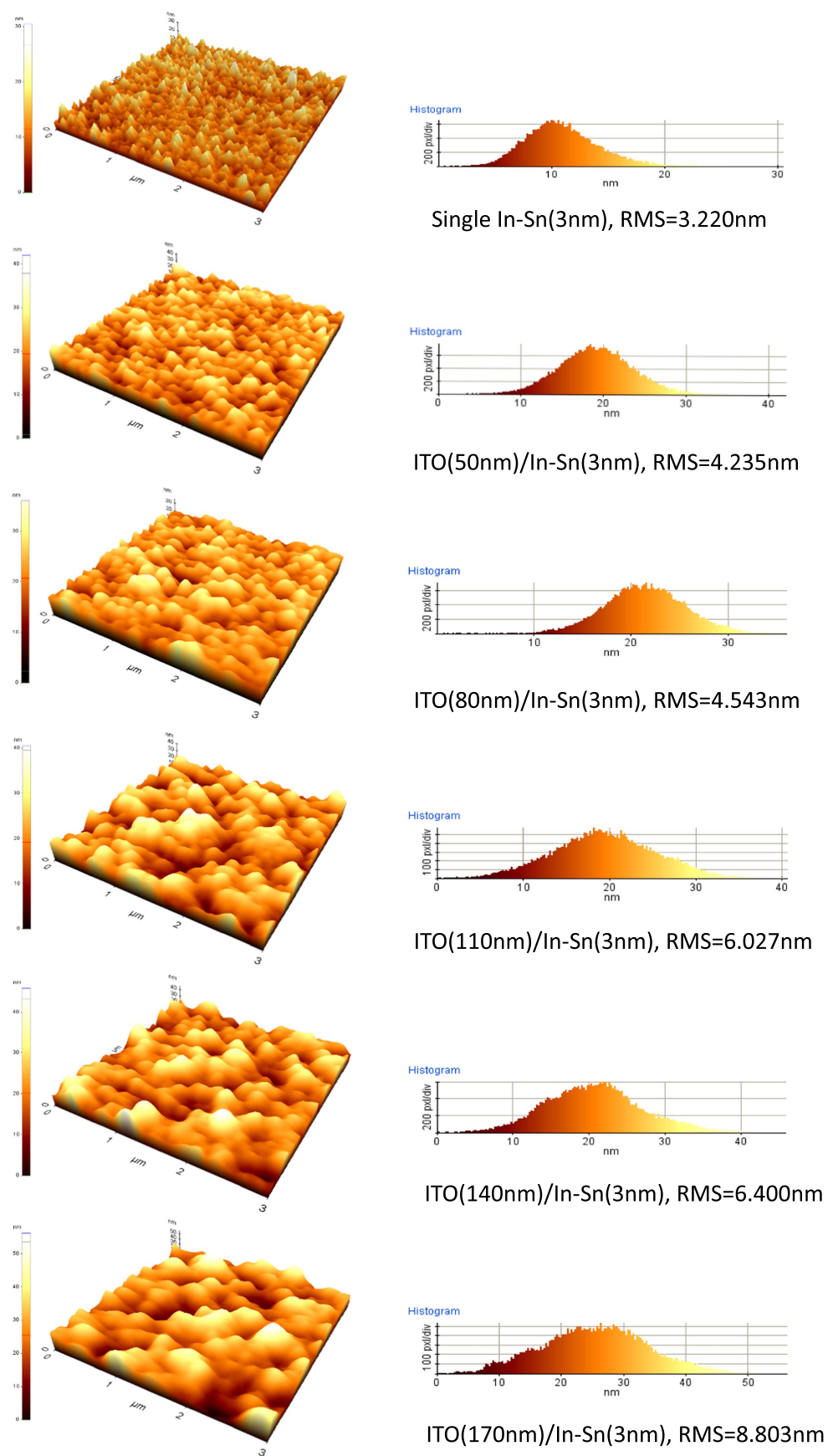


**Figure 3.** Representative AFM images and their corresponding grain height distributions (right column) of ITO/In-Sn NPs as a function of ITO thickness.

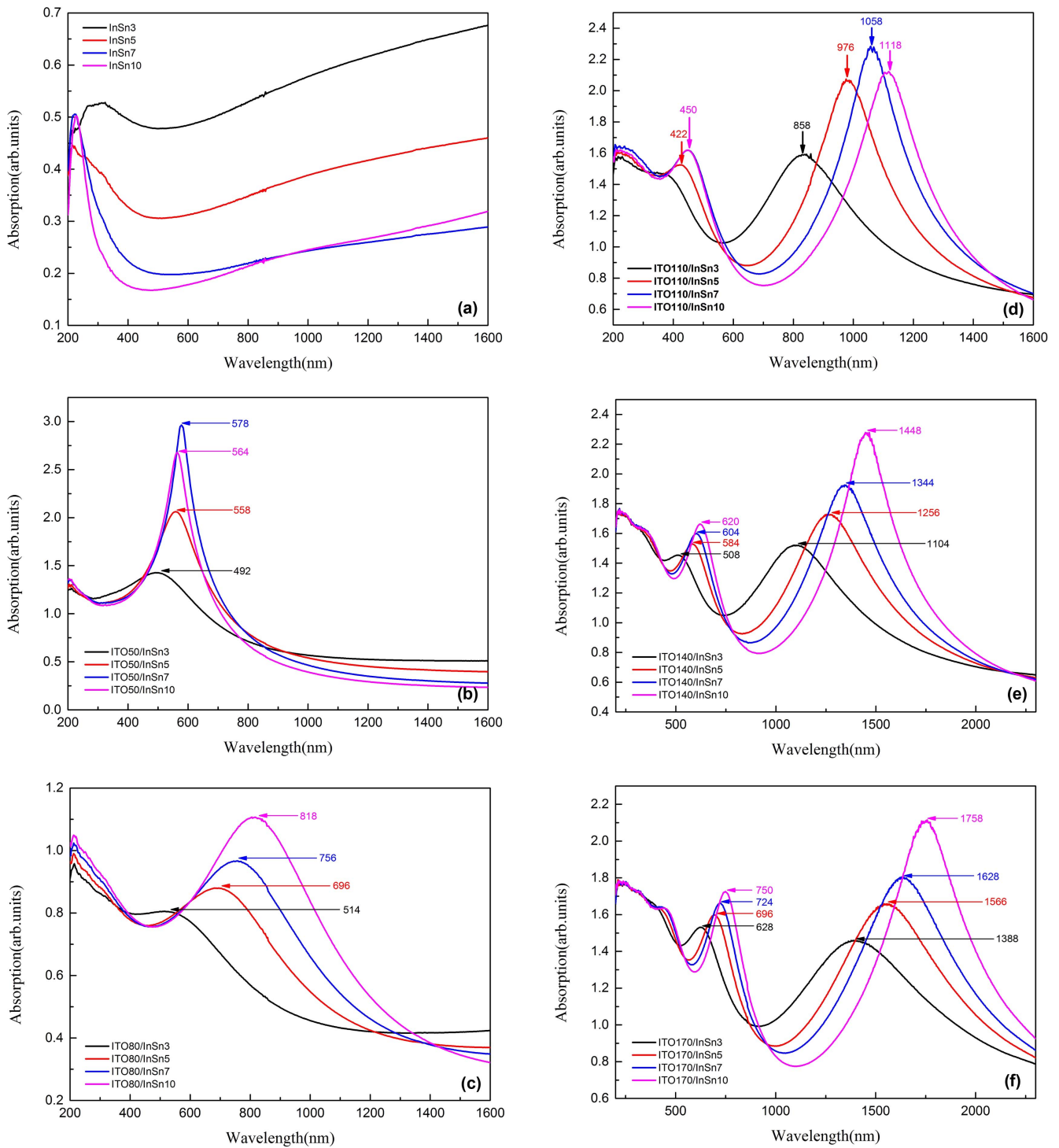


**Figure 4.** The LSPR of ITO in an ITO/In-Sn bilayer structure. Each group has four samples; the thickness of the In-Sn layer was always 3, 5, 7 and 10 nm for a fixed ITO thickness.

analytical performance. Therefore, in the ITO/In-Sn bilayer structure, the LSPR wavelength of In-Sn and ITO NPs can be well tuned from the UV to the visible region and from the NIR to the IR region, respectively, by simply engineering the thickness of ITO/In-Sn structure. This finding also provides a wide range of opportunities for realizing plasmonic materials, making them suitable for NIR LSPR sensing, especially in biosensing applications [49, 50].

In LSPR biosensing applications, one of the important characteristics is stability. Therefore, we study the aging of ITO/In-Sn films in ambient air exposure to evaluate the stability of ITO LSPR. Figure 6(a) shows the LSPR spectrum of the as-deposited ITO samples and after 15 d and 30 d exposure to ambient air. Take ITO(110 nm)/In-Sn(3 nm) as an example (figure 3(a)): the absorption spectrum shows an obvious blue shift with an enhanced absorption peak at

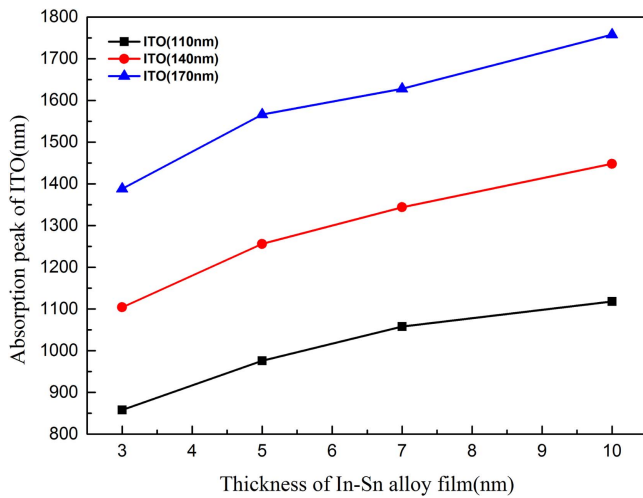


**Figure 5.** The LSPR wavelength shift of ITO NPs as a function of the In-Sn alloy film.

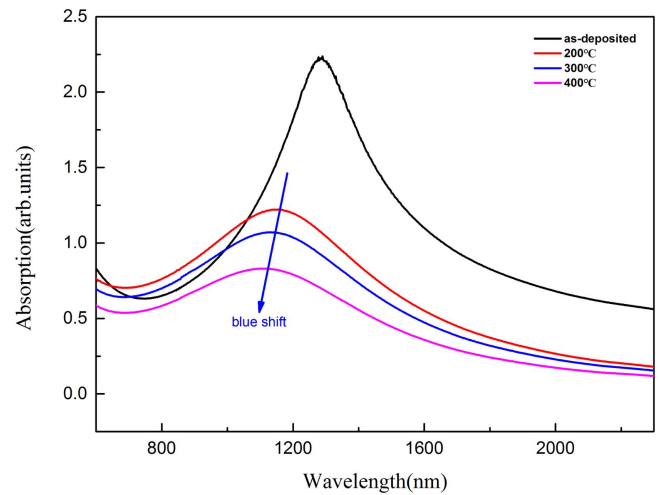


**Figure 7.** A representative sample of ITO(140 nm)/In-Sn(5 nm) for the LSPR shift of ITO NPs after vacuum annealing.

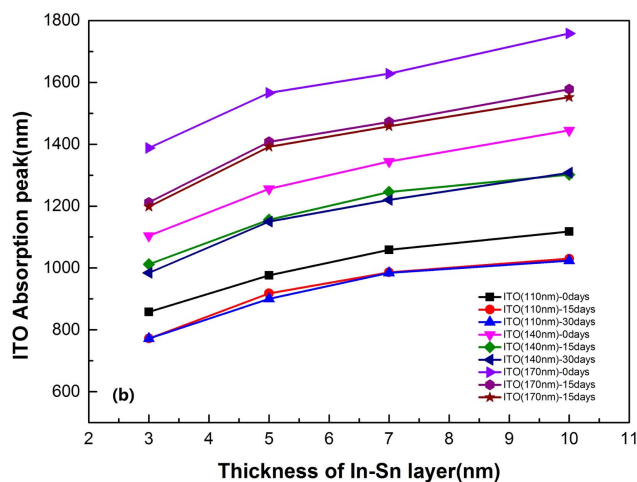
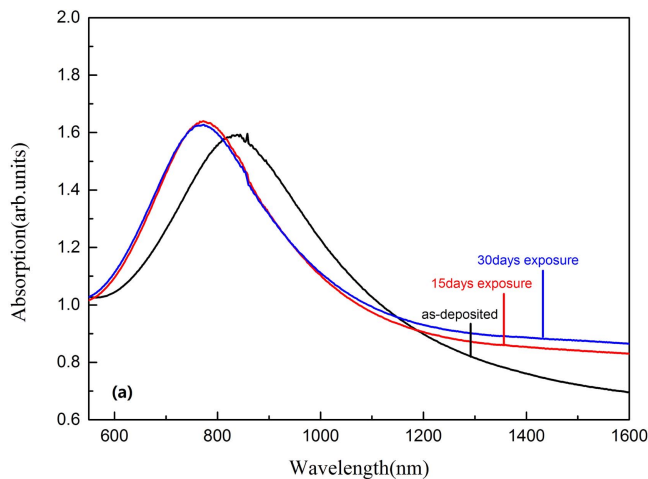


**Figure 6.** The LSPR wavelength shift of ITO NPs in air exposure for 15 d and 30 d: (a) a representative sample of ITO(110 nm)/In-Sn(3 nm) for LSPR shift; (b) the LSPR shift for all samples after air exposure.

around 800 nm after 15 d exposure, while the spectrum shows a slight difference with the exposure time increasing to 30 d. For other samples, the variations of ITO LSPR exposed to air are shown in figure 6(b). Similarly to ITO(110 nm)/In-Sn

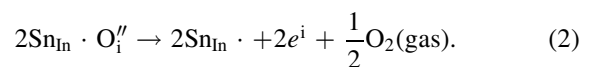
(3 nm), initially the ITO LSPR is blue-shifted after 15 d exposure and then stays almost unchanged after 30 d exposure in air, demonstrating that in our experiment the ITO/In-Sn structure possesses good stability, which is desired in practical LSPR sensor applications.

### 3.4. Vacuum annealing effect on the ITO LSPR

According to equation (1), the LSPR frequency  $\omega$  varies as the square root of the free carrier concentration, where  $m^*$  is the effective mass of an electron,  $\epsilon$  is the vacuum permittivity and  $e$  is the electron charge [51]

$$\omega = \sqrt{\frac{ne^2}{m^*\epsilon_0}} \quad (1)$$

In other words, one can tune the LSPR frequency by changing the free carrier concentration. As for ITO NPs, the free carrier concentration can be changed to tune its LSPR by thermal annealing in an oxidizing or vacuum environment. In the case of ITO, there is a route [52] for generating free electrons via annealing, as shown in equation (2) [53]:



Consequently, oxygen vacancy formation is expected to be preferred and thus leads to a higher free-electron concentration by annealing in a reducing atmosphere or low ambient oxygen partial pressure (such as the vacuum environment) [54]. Here, to demonstrate the tunability of an ITO LSPR through the carrier concentration adjustment, amorphous ITO NPs were annealed for 20 min in a vacuum environment with a base pressure of  $7.0 \times 10^{-4}$  Pa and an annealing temperature of 200 °C, 300 °C and 400 °C, respectively. Figure 7 shows the representative absorption spectra of ITO LSPR in the sample ITO(140 nm)/In-Sn(5 nm) with a different annealing temperature under a vacuum atmosphere. A significant blue shift can be observed in the annealed samples: the absorption peak gradually shifts from 1256 to 1104 nm. According to equation (2), the increased annealing

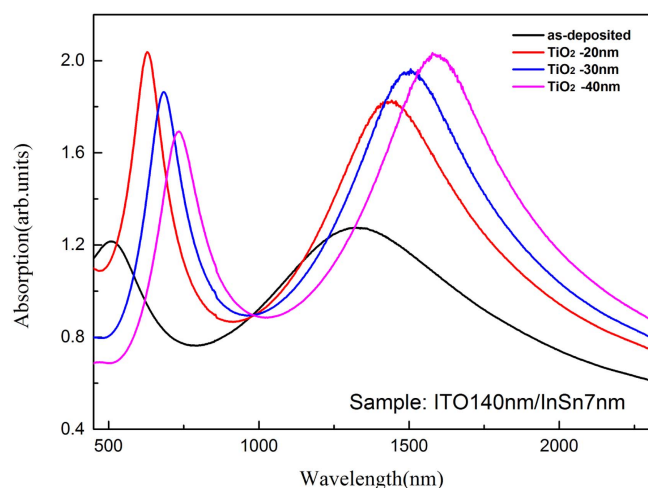


**Figure 8.** A representative sample of ITO(140 nm)/In-Sn(7 nm) for the LSPR wavelength of ITO NPs as a function of the thickness of the  $\text{TiO}_2$  layer.

temperature results in a higher free carrier concentration, leading to the blue shift of the LSPR peaks and indicating that a higher reducing atmosphere increases the dissociation of the tin-oxygen complex [55]. This confirms that the LSPR absorption peaks of ITO NPs can be well and effectively tuned by controlling the annealing atmosphere.

### 3.5. Sensitivity to the refractive index of the surrounding media

As applications for LSPR sensors, it is of great importance to understand the dependence of LSPR frequency on the refractive index of the surrounding medium. The LSPR wavelength is known to be affected by the refractive index of the surrounding medium [21, 56]. Taking advantage of this unique phenomenon, it is possible to use the ITO layer to sense the index  $n$  change of their environment. To perform such a study, we deposited other samples of ITO(140 nm)/In-Sn(7 nm) covered with thin  $\text{TiO}_2$  ( $n = 2.3$ ) layers of different thickness. Figure 8 shows the LSPR shifts of representative ITO/In-Sn samples as a function of the  $\text{TiO}_2$  layer thickness. According to Mie's theory, the plasmon materials that are surrounded by a medium with a higher refractive index are expected to have a lower LSPR frequency. As plotted in this figure, red shifts are clearly observed in the samples coated with the thin  $\text{TiO}_2$  layer compared with the as-deposited one ( $n = 1$  of air). Also, both LSPR peak intensities of In-Sn and ITO NPs are enhanced after deposition of the  $\text{TiO}_2$  layer. Interestingly, the variation tendency of both enhanced LSPR peaks are contrasting: the former shows sign of abating while the latter improves as the  $\text{TiO}_2$  thickness increases. With the top  $\text{TiO}_2$  layer, the changed surrounding medium enables the In-Sn NPs to interact strongly with the ITO layer, resulting in an enhanced absorption intensity. A thicker  $\text{TiO}_2$  layer, however, inhibits the LSPR coupling between the In-Sn and ITO NPs, thus depressing the absorption intensity of In-Sn. As for the ITO LSPR peak, the thicker  $\text{TiO}_2$  layer is expected to increase the near field electric field intensity, leading to a further shift in the LSPR wavelength, thus enhancing the

absorption intensity. On balance, these results demonstrate that the LSPR in the ITO/In-Sn structure has good sensitivity and can be considered for application in LSPR sensing.

## 4. Conclusions

In summary, the LSPR properties of both ITO and In-Sn NPs in ITO/In-Sn bilayers were investigated. The LSPR wavelength of In-Sn NPs can be tuned from UV to the visible region. In particular, our findings show that the LSPR wavelength peak of ITO NPs can be well tuned from 858 to 1758 nm by simply engineering the thickness of the ITO/In-Sn bilayer. Due to the higher free carrier concentration, the blue shift of ITO LSPR can be observed in the annealed sample, indicating that the LSPR of ITO in the ITO/In-Sn structure can also be tuned through vacuum annealing. These findings provide a simple and cost-effective way to effectively tune the LSPR of ITO NPs. As an example for LSPR sensors, the ITO/In-Sn film is demonstrated to have both good stability and sensitivity, which might play a significantly important role in the development of practical applications of photonics and optoelectronics.

## Acknowledgments

This work was partially supported by the National Key Research and Development Program of China (2016YFB1102303) and the National Natural Science Foundation of China (61775140, 61775141).

## ORCID iDs

Wenzuo Wei  <https://orcid.org/0000-0002-3880-3576>

## References

- [1] Gaspar D *et al* 2013 Influence of the layer thickness in plasmonic gold nanoparticles produced by thermal evaporation *Sci. Rep.* **3** 1469
- [2] Verma S, Rao B T, Detty A P, Ganesan V, Phase D M, Rai S K, Bose A, Joshi S C and Kukreja L M 2015 Surface plasmon resonances of Ag-Au alloy nanoparticle films grown by sequential pulsed laser deposition at different compositions and temperatures *J. Appl. Phys.* **117** 133105
- [3] Haes A J and Van Duyne R P 2011 A unified view of propagating and localized surface plasmon resonance biosensors *Anal. Bioanal. Chem.* **379** 920–30
- [4] Zhu C H, Meng G W, Huang Q, Zhang Z, Xu Q L, Liu G Q, Huang Z L and Chu Z Q 2011 Ag nanosheet-assembled micro-hemispheres as effective SERS substrates *Chem. Commun.* **47** 2709–11
- [5] West J L and Halas N J 2003 Engineered nanomaterials for biophotonics applications: improving sensing, imaging, and therapeutics *Annu. Rev. Biomed. Eng.* **5** 285–92
- [6] Atwater H A and Polman A 2010 Plasmonics for improved photovoltaic devices *Nat. Mater.* **9** 205–13

- [7] Bakker R M, Yuan H K, Liu Z, Drachev V P, Kildishev A V, Shalaev V M, Pedersen R H, Gresillon S and Boltasseva A 2008 Enhanced localized fluorescence in plasmonic nanoantennae *Appl. Phys. Lett.* **92** 043101
- [8] Mühlischlegel P, Eisler H J, Martin O J F, Hecht B and Pohl D W 2005 Resonant optical antennas *Science* **308** 1607–9
- [9] Yang Y, Nogami M, Shi J L, Chen H R, Ma G H and Tang S H 2006 Controlled surface-plasmon coupling in SiO<sub>2</sub>-coated gold nanochains for tunable nonlinear optical properties *Appl. Phys. Lett.* **88** 081110
- [10] Zheng X L, Xu W Q, Corredor C, Xu S P, An J, Zhao B and Lombardi J R 2007 Laser-induced growth of monodisperse silver nanoparticles with tunable surface plasmon resonance properties and a wavelength self-limiting effect *J. Phys. Chem. C* **111** 14962–7
- [11] Bouhelier A, Bachelot R, Lerondel G, Kostcheev S, Royer P and Wiederrecht G P 2005 Surface plasmon characteristics of tunable photoluminescence in single gold nanorods *Phys. Rev. Lett.* **95** 267405
- [12] Lakshmanan S B, Zou X, Hossu M, Ma L, Yang C and Chen W 2012 Local field enhanced Au/CuS nanocomposites as efficient photothermal transducer agents for cancer treatment *J. Biomed. Nanotechnol.* **8** 883–90
- [13] Jiang R, Li B, Fang C and Wang J 2014 Metal/semiconductor hybrid nanostructures for plasmon-enhanced applications *Adv. Mater.* **26** 5274–309
- [14] Dorfs D, Hartling T, Miszta K, Bigall N C, Kim M R, Genovese A, Falqui A, Povia M and Manna L 2011 Reversible tunability of the near-infrared valence band plasmon resonance in Cu<sub>2–x</sub>Se nanocrystals *J. Am. Chem. Soc.* **133** 11175–80
- [15] Chen P C, Mwakwari S C and Oyelere A K 2008 Gold nanoparticles: from nanomedicine to nanosensing *Nanotechnol. Sci. Appl.* **1** 45–66
- [16] You J, Zhang G and Li C 2010 Exceptionally high payload of doxorubicin in hollow gold nanospheres for near-infrared light-triggered drug release *ACS Nano* **4** 1033–41
- [17] Shakeri-Zadeh A, Ghasemifard M and Mansoori G A 2010 Structural and optical characterization of folate-conjugated gold-nanoparticles *Physica E* **42** 1272–80
- [18] Maestro L M, Haro-Gonzalez P, Del R B, Ramiro J, Caamano A J, Carrasco E, Juarranz A, Sanz-Rodriguez F, Sole J G and Jaque D 2013 Heating efficiency of multi-walled carbon nanotubes in the first and second biological windows *Nanoscale* **5** 7882–9
- [19] Tsai M F, Chang S H G, Cheng F Y, Shanmugam V, Cheng Y S, Su C H and Yeh C S 2013 Au nanorod design as light-absorber in the first and second biological near-infrared windows for *in vivo* photothermal therapy *ACS Nano* **7** 5330–42
- [20] Ma K, Zhou N, Yuan M, Li D and Yang D 2014 Tunable surface plasmon resonance frequencies of monodisperse indium tin oxide nanoparticles by controlling composition, size, and morphology *Nanoscale Res. Lett.* **9** 547
- [21] Kanehara M, Koike H, Yoshinaga T and Teranishi T 2009 Indium tin oxide nanoparticles with compositionally tunable surface plasmon resonance frequencies in the near-IR region *J. Am. Chem. Soc.* **131** 17736–7
- [22] Manthiram K and Alivisatos A P 2012 Tunable localized surface plasmon resonances in tungsten oxide nanocrystals *J. Am. Chem. Soc.* **134** 3995–8
- [23] Garcia G, Buonsanti R, Rønnerstrom E L, Mendelsberg R J, Lordes A, Anders A, Richardson T J and Milliron D J 2011 Dynamically modulating the surface plasmon resonance of doped semiconductor nanocrystals *Nano Lett.* **11** 4415–20
- [24] Buonsanti R, Lordes A, Aloni S, Helms B A and Milliron D J 2011 Tunable infrared absorption and visible transparency of colloidal aluminum-doped zinc oxide nanocrystals *Nano Lett.* **11** 4706–10
- [25] Li W et al 2013 CuTe nanocrystals: shape and size control, plasmonic properties, and use as SERS probes and photothermal agents *J. Am. Chem. Soc.* **135** 7098–101
- [26] Encina E R and Coronado E A 2011 Near field enhancement in Ag Au nanospheres heterodimers *J. Phys. Chem. C* **115** 15908–14
- [27] Sun Y, Foley J J, Peng S, Li Z and Gray S K 2013 Interfaced metal heterodimers in the quantum size regime *Nano Lett.* **13** 3958–64
- [28] Brown L V, Sobhani H, Lassiter J B, Nordlander P and Halas N J 2010 Heterodimers: plasmonic properties of mismatched nanoparticle pairs *ACS Nano* **4** 819–32
- [29] Halas N J, Lal S, Chang W S, Link S and Nordlander P 2011 Plasmons in strongly coupled metallic nanostructures *Chem. Rev.* **111** 3913–61
- [30] Luther J M, Jain J K, Ewers T and Alivisatos A P 2011 Localized surface plasmon resonances arising from free carriers in doped quantum dots *Nat. Mater.* **10** 361–6
- [31] Mendelsberg R J, Garcia G, Li H, Manna L and Milliron D J 2012 Understanding the plasmon resonance in ensembles of degenerately doped semiconductor nanocrystals *J. Am. Chem. Soc.* **116** 12226–31
- [32] Szunerits S, Castel X and Boukherroub R 2008 Preparation of electrochemical and surface plasmon resonance active interfaces: deposition of indium tin oxide on silver thin films *J. Phys. Chem. C* **112** 10883–8
- [33] Franzen S, Rhodes C, Cerruti M, Gerber R W, Losego M, Maria J P and Aspnes D E 2009 Plasmonic phenomena in indium tin oxide and ITO-Au hybrid films *Opt. Lett.* **34** 2867–9
- [34] Chen F, Fei W, Sun L, Lia Q, Di J and Wu Y 2014 Direct growth of coupled gold nanoparticles on indium tin oxide substrate and construction of biosensor based on localized surface plasmon resonance *Sensor. Actuat. B-Chem.* **191** 337–43
- [35] Xia Y, Xiong Y, Lim B and Skrabalak S E 2009 Shape-controlled synthesis of metalnanocrystals: simple chemistry meets complex physics? *Angew. Chem., Int. Ed. Engl.* **48** 60–103
- [36] Hong R, Song X, Tao C, Zhang D and Zhang D 2016 Surface-enhanced Raman scattering of silver thin films on as-roughened substrate by reactive ion etching *Appl. Phys. A* **122** 1–6
- [37] Song P, Akao H, Kamei M, Shigesato Y and Yasui I 1999 Preparation and crystallization of tin-doped and undoped amorphous indium oxide films deposited by sputtering *Jpn. J. Appl. Phys.* **38** 5224–6
- [38] Yang C H, Lee S C, Lin T C and Chen S C 2008 Electrical and optical properties of indium tin oxide films prepared on plastic substrates by radio frequency magnetron sputtering *Thin Solid Films* **516** 1984–91
- [39] Kathryn M M, Feng H, Seunghyun L, Peter N and Jason H H 2010 A single molecule immunoassay by localized surface plasmon resonance *Nanotechnology* **21** 255503
- [40] Sherry L J, Chang S H, Schatz G C, Van Duyne R P, Wiley B J and Xia Y 2005 Localized surface plasmon resonance spectroscopy of single silver nanocubes *Nano Lett.* **5** 2034–8
- [41] Mahmoud M A, Chamanzar M, Adibi A and El-Sayed M A 2012 Effect of the dielectric constant of the surrounding medium and the substrate on the surface plasmon resonance spectrum and sensitivity factors of highly symmetric systems: silver nanocubes *J. Am. Chem. Soc.* **134** 6434–42
- [42] Liu X, Jia L, Fan G, Gou J and Liu F S 2016 Au nanoparticle enhanced thin-film silicon solar cells *Sol. Energ. Mat. Sol. C* **147** 225–334

- [43] Kim S S, Choi S Y, Park C G and Jin H W 1999 Transparent conductive ITO thin films through the sol-gel process using metal salts *Thin Solid Films* **347** 155–60
- [44] Wei W, Hong R, Meng Y, Tao C and Zhang D 2017 Electron-beam irradiation induced phase transformation, optical absorption and surface-enhanced Raman scattering of indium tin alloy thin films *Superlattice. Microstruct.* **106** 189–96
- [45] Eustis S and El-Sayed M A 2006 Why gold nanoparticles are more precious than pretty gold: noble metal surface plasmon resonance and its enhancement of the radiative and nonradiative properties of nanocrystals of different shapes *Chem. Soc. Rev.* **35** 209–17
- [46] Hong R, Wang X, Ji J, Tao C, Zhang D and Zhang D 2015 ITO induced tunability of surface plasmon resonance of silver thin film *Appl. Surf. Sci.* **356** 701–6
- [47] Band B P, Peumans P and Forrest S R 2004 Long-range absorption enhancement in organic tandem thin-film solar cells containing silver nanoclusters *J. Appl. Phys.* **96** 7519–26
- [48] Xing G, Jiang J, Ying J Y and Ji W 2010 Fe<sub>3</sub>O<sub>4</sub>-Ag nanocomposites for optical limiting: broad temporal response and low threshold *Opt. Express* **18** 6183–90
- [49] Larsson E M, Alegret J, Käll M and Sutherland D S 2007 Sensing characteristics of NIR localized surface plasmon resonances in gold nanorings for application as ultrasensitive biosensors *Nano Lett.* **7** 1256–63
- [50] Ye J, Dorpe P V, Lagae L, Maes G and Borghs G 2009 Observation of plasmonic dipolar anti-bonding mode in silver nanoring structures *Nanotechnology* **20** 465203
- [51] Link S and El-Sayed M A 1999 Spectral properties and relaxation dynamics of surface plasmon electronic oscillations in gold and silver nanodots and nanorods *J. Phys. Chem. B* **103** 8410–26
- [52] Freeman A J, Poepelmeier K R, Mason T O, Chang R P H and Marks T J 2000 Chemical and thin-film strategies for new transparent conducting oxides *MRS Bull.* **25** 45–51
- [53] Kröger F A and Vink H J 1958 Relations between the concentrations of imperfections in crystalline solids *J. Phys. Chem. Solids* **3** 208–23
- [54] Li S Q, Guo P, Zhang L, Zhou W, Odom T W, Seideman T, Ketterson J B and Chang R P H 2011 Infrared plasmonics with indium tin-oxide nanorod arrays *ACS Nano* **5** 9161–70
- [55] Tuo Y, Wu Y, Huang M, Wang K, Huang Y, Zhou Z and She S 2015 The surface plasmon resonance absorption of indium tin oxide nanoparticles and its control *Adv. Mater. Res.* **1118** 160–5
- [56] Shi W, Zeng H, Sahoo Y, Ohulchanskyy T Y, Ding Y, Wang Z, Swihart M and Prasad P N 2006 A general approach to binary and ternary hybrid nanocrystals *Nano Lett.* **6** 875–81